Double resonant Raman scattering and photoluminescence mediated by heavy and light hole excitons in a (Cd, Mn)Te quantum well in external magnetic field

N. V. Kozyrev [1,*] I. I. Kozlov [1] B. R. Namozov [1] L. E. Golub [1] M. M. Glazov [1,2]
Yu. G. Kusrayev,[1] and T. Wojtowicz [3]

[1]*Ioffe Institute, Russian Academy of Sciences, 194021 St. Petersburg, Russia*
[2]*Higher School of Economics, National Research University, 194100 St. Petersburg, Russia*
[3]*International Research Centre MagTop, Institute of Physics, Polish Academy of Sciences, PL-02668 Warsaw, Poland*

We study exciton-mediated double resonant Raman scattering via longitudinal optical (LO) phonons in a diluted magnetic (Cd, Mn)Te/(Cd, Mg)Te quantum well. Experiments performed at 1.5 K in external magnetic field in Faraday geometry reveal strong enhancement of the LO phonon Raman line emission from the lower Zeeman sublevel of the heavy hole exciton if the upper Zeeman sublevel of either the light hole exciton or the heavy hole exciton is exactly the longitudinal optical phonon energy above the exciton ground state. In these cases a double resonance condition is satisfied, with the ingoing resonance being either the light or heavy hole exciton upper Zeeman sublevel and the outgoing resonance being the heavy hole exciton lower Zeeman sublevel. We discuss the mechanisms of the effect and demonstrate the importance of the exchange interaction in the exciton resulting in the mixing of heavy and light hole excitons active in the same circular polarization as well as the deformation-optical hole-phonon interaction. This double resonance condition can be effectively reached by varying the magnetic field applied to the quantum well. We provide theoretical arguments supporting the absence of the spin-conserving light to heavy exciton double resonant Raman scattering in experiments. We also discuss the difference between photoluminescence and resonant Raman scattering in our system with significant inhomogeneous broadening.

I. INTRODUCTION

One of the techniques used for the study of the electron-phonon interaction in semiconductors is resonant Raman scattering. It manifests itself as a sharp increase in the Raman features in the secondary radiation spectra when the incident photon energy is close to the electron excitation energies of a studied structure. Two types of resonances are known: an ingoing resonance and an outgoing resonance. The former occurs when incident light energy is tuned to coincide with the energy of an exciton state. Strong electron-phonon interaction results in the excitation of vibrations of the crystal lattice of different modes. Due to the strong electron-phonon interaction in materials with polar covalent bounds like CdTe, longitudinal optical (LO) phonons are created in this process. The outgoing resonance occurs when the photoexcitation energy is tuned by an LO energy higher than the exciton energy, which also leads to the increase of the Raman scattering intensity. It is possible to prepare a material system in which the ingoing and outgoing resonance conditions are achieved simultaneously. This situation is called double resonant Raman scattering (DRRS). DRRS is used as a powerful technique to study the electronic and vibrational properties of solid states; for example, it is commonly used nowadays to study two-dimensional structures like graphene and transition metal dichalcogenides (see Refs. [1–3] and references therein).

There are several ways to reach the DRRS conditions. In bulk materials, for example, it is possible to split heavy and light hole exciton states by a uniaxial stress [4]. One can study a semiconductor quantum well (QW), in which a careful choice of the width and the depth parameters leads to the quantization of the exciton states which satisfy the DRRS conditions [5]. Doping a semiconductor with magnetic ions (e.g., manganese) helps in the study of the DRRS since the strong exchange interaction between magnetic ions and free charge carriers leads to the giant Zeeman splitting of the exciton states being comparable to LO phonon energy in some moderate magnetic fields. For example, in Ref. [6] the DRRS in bulk (Cd, Mn)Te was observed between the light and heavy hole exciton states split in the external magnetic field. One can combine those two approaches and investigate the DRRS phenomenon in diluted magnetic semiconductor (DMS; a semiconductor doped with magnetic ions) QWs, like what was done in Ref. [7], where the DRRS between $1s$ and $2s$ exciton states was studied. The DRRS between exciton states with different angular momentum projections should inevitably lead to fast spin relaxation processes. Experimentally, this was studied in the DMS-based (Zn, Mn)Se/CdSe superlattice reported in Ref. [8]. It was shown there that, indeed, the DRRS between heavy hole exciton states with different angular momentum projections leads to the fast spin relaxation.

In the papers mentioned above, DRRS between the states of light and heavy hole excitons with different projections of angular momentum [6] and between heavy hole exciton states

*kozyrev.nikolay@bk.ru

245306-1

with different projections [8] were studied independently. In this paper we report on the experimental and theoretical study of the efficiencies of these two cases of DRRS combined for light and heavy exciton states with different projections of the angular momentum in the (Cd, Mn)Te QW. The relation between the intensities of the resonant Raman line and inhomogeneously broadened photoluminescence is also discussed.

This paper is organized as follows. Experimental results are presented in Sec. II. In Sec. II A we present the experimental results for the resonant Raman scattering in different magnetic fields. Then in Sec. II B we present additional experimental results for the photoluminescence (PL) and photoluminescence excitation (PLE) spectroscopy to determine the magnetic field values where the DRRS should be observed. Theory is presented in Sec. III. There we first study the selection rules for the LO phonon assisted DRRS and PL in quantum well structures (Sec. III A); afterwards, we present the microscopic mechanisms of the DRRS (Secs. III B, III C, and III D) and then discuss the interplay of the DRRS and PL in the presence of inhomogeneous broadening (Secs. III E, III F, and III G). The obtained results are discussed in Sec. IV, and Sec. V summarizes our studies.

II. EXPERIMENTAL RESULTS

A. Resonant Raman scattering with LO phonon emission

The studied sample (041700A) is a structure with three epitaxial QWs of $Cd_{0.97}Mn_{0.03}Te$ DMS with 40, 60, and 100 Å widths separated from each other by a nonmagnetic barrier of $Cd_{0.76}Mg_{0.24}Te$ of 300 Å width. PL spectra and resonant Raman scattering (RRS) spectra with LO phonon emission were detected with a triple spectrometer with a spectral resolution of 50 μeV and a CCD camera. A tunable Ti: sapphire laser with a spectral width of about 0.1 μeV was used as a photoexcitation source. The laser power was fixed at 1 mW and was focused on the sample to a spot of 300 μm diameter. The studies were carried out on a 100 Å wide QW at a temperature of 1.5 K in magnetic field in the Faraday geometry. The choice of the sample is determined by two factors. First, a 3% molar manganese concentration causes giant exciton spin splitting comparable to the LO phonon energy in moderate magnetic fields. Second, the influence of the fluctuations of the QW width on the inhomogeneous broadening of the exciton PL is reduced in a 100 Å wide QW.

In the absence of magnetic field, the PL spectra of the studied structure exhibit two overlapping bands corresponding to the inhomogeneously broadened PL of heavy hole excitons (X, width ∼3 meV) and the electron (negatively charged) trion (T, width ∼6 meV; the sign of the trion was established in Ref. [9] on a very similar sample with 1% manganese concentration). Exciting the sample with the photons energetically exceeding the exciton PL by approximately $\hbar\Omega_{LO} = 21$ meV (LO phonon energy), one can observe an additional narrow line (width is about 0.4 meV) in the spectra which correspond to RRS with LO phonon emission [see Fig. 1(a)]. The intensity of the LO line shows a resonance behavior depending on the photoexcitation energy. The maximum of the resonance contour is achieved when the LO line is near the maximum
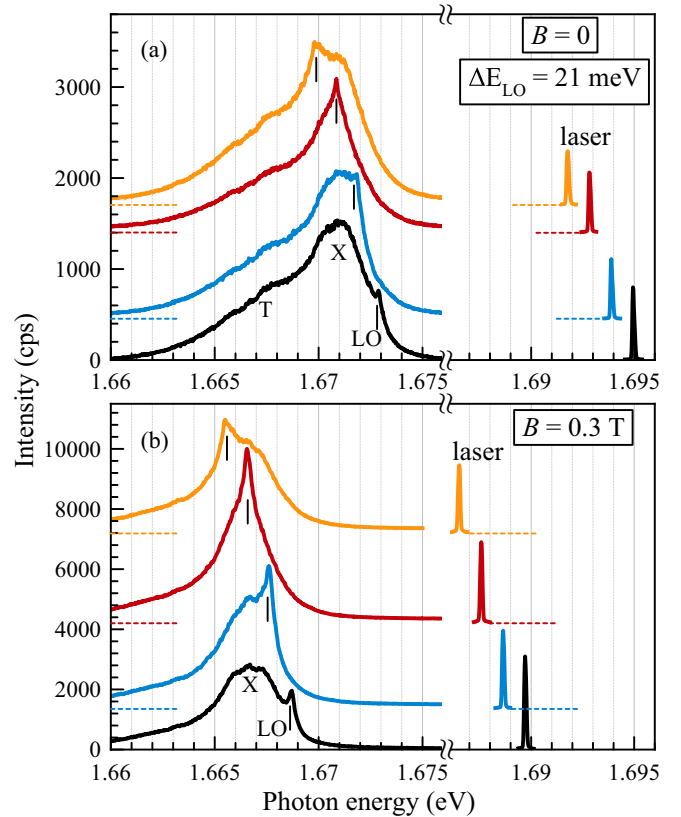

FIG. 1. The spectra of the secondary emission of the 100 Å wide QW under the photoexcitation near the outgoing resonance of Raman scattering with the LO phonon emission in the magnetic fields (a) $B = 0$ and (b) $B = 0.3$ T. LO denotes the RRS line; X and T denote the bands of the inhomogeneously broadened exciton and negatively charged trion PL, respectively. All the spectra are shifted vertically for clarity. Horizontal dashed lines show the zero-intensity level for each spectrum. $T = 1.5$ K.

of the exciton PL as a result of the outgoing resonance of the Raman scattering.

Under application of an external magnetic field, the inhomogeneously broadened PL spectra experience a giant Zeeman shift, which is typical for DMS-based systems [10]. In addition, the intensity of the trion PL decreases with the increase of the magnetic field, which can be attributed to the destabilization of the singlet trion state in the magnetic field [11,12]. The ground state of the Zeeman doublet of the exciton and trion emits light in σ^+ polarization. It was observed that increasing the magnetic field up to 0.3 T and exciting with the light of σ^- polarization in the outgoing resonance condition, the intensity of the LO line increases by a factor of 6 compared to the zero magnetic field case [Fig. 1(b)]. With a further increase of the magnetic field, the LO line intensity showed a nonmonotonic decrease.

For a thorough analysis of the LO line intensity magnetic field dependence we had to extract the feature of RRS superimposed on the PL in the secondary emission spectra and plot its dependence on the photoexcitation energy. For that we exploited the fact that, for each given magnetic field value, the shape and energy position of the inhomogeneously broadened PL practically do not depend on the photoexcitation energy
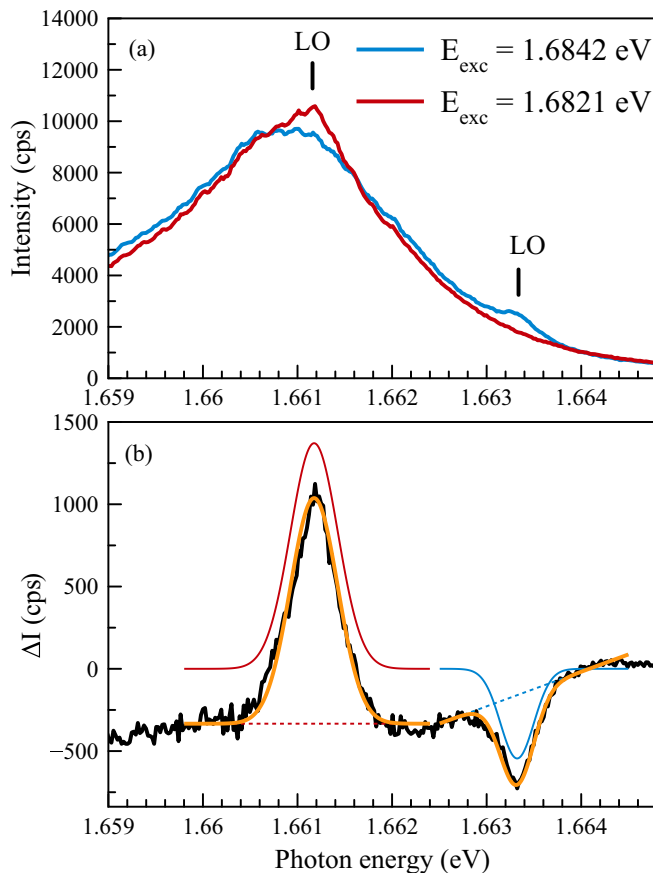
FIG. 2. (a) Two spectra measured in $B = 0.7$ T under photoexcitation with different photon energies. (b) The black curve represents the difference (ΔI) between spectra shown in (a). Solid colored lines are Gaussian contours used for the LO line approximation; dashed colored lines are used to subtract a baseline left after the subtraction. The orange solid line represents the sum of the Gaussian contour and the baseline. $T = 1.5$ K.
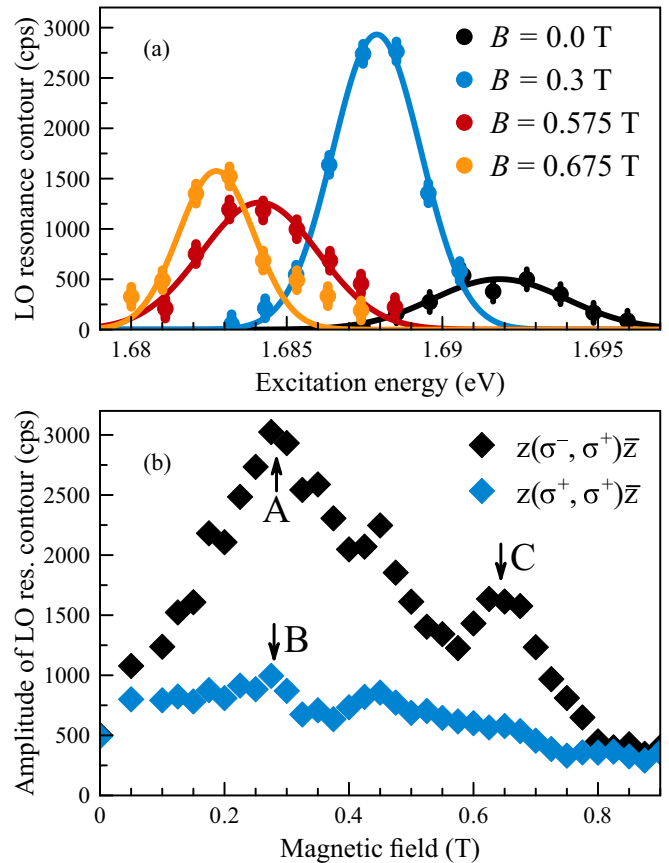

FIG. 3. (a) Symbols represent resonance contours of RRS with LO phonon emission in different magnetic fields in the $z(\sigma^-, \sigma^+)\bar{z}$ configuration. Error bars are estimated as ± 100 counts per second. Solid lines are guides for the eye. The DRRS conditions are satisfied at $B \approx 0.3$ T and $B \approx 0.65$ T. (b) Magnetic field dependence of the amplitudes of the Raman scattering resonance contour. Error bars are within the symbol size. A, B, and C correspond to the DRRS conditions derived in Sec. II B and in Fig. 4. $T = 1.5$ K.

[an example of two typical spectra measured at different excitation energies is shown in Fig. 2(a)]. Therefore, subtracting two spectra measured at different energies of excitation, we could almost completely remove the contributions of the exciton and trion PL from the spectra, leaving the intensity of the LO line unchanged [see Fig. 2(b)]. Using the sum of the Gaussian contour and a linear function for the approximation, we managed to deduce the dependence of the LO line intensity (Gaussian contour's amplitude) on the excitation energy and therefore obtain a resonance contour for each value of the external magnetic field.

Figure 3(a) shows outgoing resonance contours of the Raman scattering obtained with this extraction procedure in the $z(\sigma^-, \sigma^+)\bar{z}$ polarization configuration for several magnetic fields. The width of the Raman scattering resonance contour does not strongly depend on the magnetic field and has the same order of magnitude as the exciton PL (about 3 meV).

The magnetic field dependence of the Raman scattering resonance contour amplitude in the cross-polarized $z(\sigma^-, \sigma^+)\bar{z}$ configuration shown in Fig. 3(b) exhibits two clear maxima at $B = 0.3$ T and $B = 0.65$ T and a faint feature at $B = 0.45$ T. The effect in the copolarized $z(\sigma^+, \sigma^+)\bar{z}$

configuration is not as pronounced as that measured in the cross polarizations; however, there is a minor increase in the amplitude of the Raman scattering resonance contours near $B = 0.25$–0.3 T and near $B = 0.45$ T.

The DRRS with LO phonon emission defines the behavior of the Raman scattering resonance contour in the magnetic field. This phenomenon consists of significant amplification of the LO line intensity in conditions in which the photoexcitation energy and the energy position of the LO line are both in resonance with the exciton states in the crystal. In the following section we identify the exciton states involved in DRRS.

B. Photoluminescence and photoluminescence excitation

In order to show which states of the exciton of the studied structure are responsible for the DRRS and in which magnetic fields it occurs, it is necessary to know the dependences of the energetic shifts of the exciton states in the magnetic field. In the simplest form the energies of the exciton states in a DMS-based QW subjected to magnetic field could be considered as combinations of the energetic shifts of the electron and hole

states. In the Faraday geometry those shifts are represented as follows (Zeeman splitting unrelated to the manganese magnetization is neglected):

$$\Delta E_{e,\pm 1/2} = \pm \tfrac{1}{2} N_0 \alpha x_{Mn} \langle S_{Mn} \rangle,$$

$$\Delta E_{hh,\pm 3/2} = \pm \tfrac{1}{2} N_0 \beta x_{Mn} \langle S_{Mn} \rangle,$$

$$\Delta E_{lh,\pm 1/2} = \Delta_{hh-lh} \pm \tfrac{1}{6} N_0 \beta x_{Mn} \langle S_{Mn} \rangle. \quad (1)$$

Here $N_0\alpha = 0.22$ eV and $N_0\beta = -0.88$ eV are the constants of the exchange interaction of manganese ions with the electrons and holes, respectively; Δ_{hh-lh} is a splitting of the light and heavy hole states in the QW, and x_{Mn} is the effective molar part of the manganese ions in the structure. The magnetic field dependence of the energetic shifts of these states is described by the Brillouin function $B_S(y)$ contained in the average spin of the manganese ions:

$$\langle S_{Mn} \rangle = S B_S \left(\frac{S \mu g B}{k(T + T_0)} \right). \quad (2)$$

Here $S = 5/2$ is the spin of a manganese magnetic ion combined from five electrons in d orbitals, μ is the Bohr magneton, $g = 2$ is the g factor of the d electrons, k is the Boltzmann's constant, B is the magnetic field strength, T is the temperature of the sample, and T_0 is a contribution to the temperature caused by the antiferromagnetic interaction between neighboring manganese ions.

The phenomenological parameters T_0, x_{Mn}, and Δ_{hh-lh} define the dependence of the energy shifts of the exciton states for the particular system. In our case the splitting Δ_{hh-lh} was derived from the exciton PLE spectrum shown in the Fig. 4(a). The PLE spectrum is deduced from the series of the PL spectra measured at different excitation energies with subsequent approximation with two Gaussian contours corresponding to the exciton and trion PL. The value of the parameter $\Delta_{hh-lh} = 16$ meV obtained from the experiment is in agreement with the simple estimations from the solution of the Schrödinger equation for particles with light and heavy hole effective masses in the symmetrical QW. Additional features in the PLE spectrum seen at energies higher than the light hole exciton are due to the excited states of the exciton and the states from the QW with a 60 Å width.

Two remaining parameters, namely, x_{Mn} and T_0, were derived from the magnetic field dependence of the σ^+ heavy hole exciton energy shift measured up to $B = 6$ T [the linear part of it is shown as the blue curve in Fig. 4(b)]. The behavior of this dependence is described by Eq. (1) as $E_0 + \Delta E_{e,-1/2} + \Delta E_{hh,+3/2}$, where E_0 is the heavy hole exciton energy in $B = 0$. This allowed us to determine the values of the parameters $x_{Mn} = 2.46\%$ and $T_0 = 2.0$ K.

Given the parameters determined above, we have calculated the energy shifts of the other three exciton states optically active in the Faraday geometry [see black curves in Fig. 4(b)]. According to this calculation, the splitting of the exciton states matches the LO phonon energy $\hbar\Omega_{LO} = 21$ meV at the magnetic field values corresponding to the maxima observed in Fig. 3(b) (all but the one in $B = 0.45$ T). The main maximum near $B = 0.35$ T corresponds to the DRRS between the light hole exciton state with an angular momentum projection of -1 and the heavy hole exciton state with a
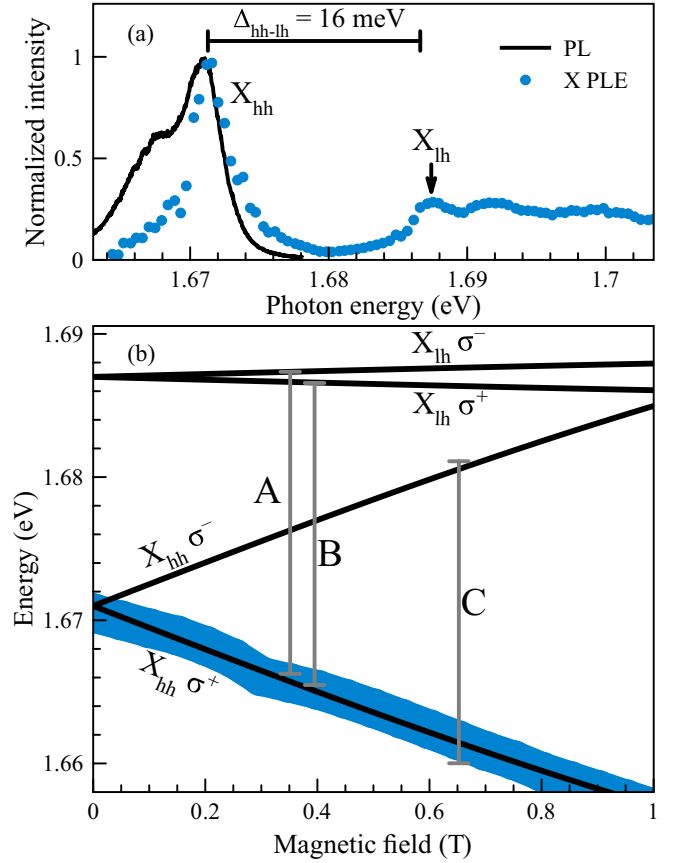

FIG. 4. (a) The blue dots represent a spectrum of the exciton PL excitation. The black curve represents the PL spectrum detected under 532 nm cw laser excitation. $B = 0$. (b) The blue curve represents the magnetic field dependence of the energy position of the heavy hole exciton PL (σ^+) in the Faraday geometry. The curve's width is 3 meV, which corresponds to the width of the exciton PL. Calculated estimations of the energy shifts of the other three exciton states optically active in the Faraday geometry. X_{lh} and X_{hh} denote that the exciton states bind to the light and heavy holes, respectively; σ^+ and σ^- correspond, respectively, to the $+1$ and -1 angular momentum projections of the exciton. $T = 1.5$ K.

projection of $+1$ [case A in Fig. 4(b)]. The additional maximum observed near $B = 0.65$ T is attributed to the double resonance between the states of the heavy hole exciton with different angular momentum projections split in the magnetic field [case C in Fig. 4(b)]. Both maxima are observed in the $z(\sigma^-, \sigma^+)\bar{z}$ polarization configuration and are clearly seen in the experiment. On the other hand, from the analysis of the magnetic field dependences, one could also expect to observe the double resonance between the light hole and heavy hole exciton states with the same angular momentum projections of $+1$ [case B in Fig. 4(b)]. However, the results presented for the copolarized $z(\sigma^+, \sigma^+)\bar{z}$ configuration show less pronounced magnetic field dependence of the amplitude of the LO line resonance contour.

III. THEORY

A. Selection rules and models of cases A and C in DRRS

Now we turn to a theoretical description of our findings. We consider an exciton in a QW made of II-VI

semiconductors. For a structure grown along the $z \parallel [001]$ axis the point symmetry could be either D_{2d} in the case of a symmetric heteropotential or C_{2v} if asymmetry is present. We assume that the heavy-light hole splitting in the structure is considerable: $\Delta_{\mathrm{hh-lh}}$ exceeds the exciton binding energy. Thus, there are well-defined excitonic states corresponding to the heavy and light holes bound with the electron. The exciton spin state is characterized by the electron spin z component $s_z = \pm 1/2$ and the hole total angular momentum z components $J_z = \pm 3/2$ for the heavy hole excitons X_{hh} and $J_z = \pm 1/2$ for the light hole exciton.

For the normal incidence of radiation, the optically active states in circular polarizations σ^+ and σ^- of X_{hh} correspond to the electron-hole pairs

$$\sigma^\pm: \quad s_z = \mp 1/2, \quad J_z = \pm 3/2 \tag{3a}$$

and

$$\sigma^\pm: \quad s_z = \pm 1/2, \quad J_z = \pm 1/2 \tag{3b}$$

for X_{lh}. In the case of experimentally studied DRRS in the configuration $z(\sigma^-, \sigma^+)\bar{z}$ the initial state is either the X_{lh} or X_{hh} active in the σ^- polarization, and the final state is the X_{hh} active in the σ^+ polarization for cases A and C [see Fig. 4(b)], respectively.

Let us assume that the charge carriers are strongly confined along the QW growth axis and the exciton as a whole can be localized by the fluctuation potential of the QW. Then the exciton wave functions take the form

$$\Psi_n(\mathbf{r}_e, \mathbf{r}_h) = \Phi_n(\mathbf{r}_e, \mathbf{r}_h)|s_z, J_z\rangle, \tag{4}$$

where $\mathbf{r}_e$ and $\mathbf{r}_h$ are the electron and hole position vectors, $\Phi_n(\mathbf{r}_e, \mathbf{r}_h)$ is the smooth envelope, and $|s_z, J_z\rangle$ is the two-particle Bloch function. Subscript n enumerates the exciton states.

The composite matrix element describing the DRRS process takes the form

$$M_{nm}^{\mathrm{DRRS}}(\mathbf{q}) = \frac{M_n^* V_{nm}^{\mathrm{LO}}(\mathbf{q}) M_m}{(\hbar\omega_i - E_m)(\hbar\omega_i - \hbar\Omega_{\mathrm{LO}} - E_n)}, \tag{5}$$

where the subscripts m and n denote, respectively, the initial exciton state created by the incident photon with frequency ω_i and the final exciton state after the LO phonon scattering; M_m and M_n are the corresponding optical transition matrix elements; and $V_{nm}^{\mathrm{LO}}(\mathbf{q})$ is the appropriate exciton-phonon interaction matrix element, with $\mathbf{q}$ being the phonon wave vector and Ω_{LO} being the LO phonon frequency. The photon scattering rate is given by Fermi's golden rule:

$$W^{\mathrm{DRRS}} = \frac{2\pi}{\hbar} \sum_{nm,\mathbf{q}} \left| M_{nm}^{\mathrm{DRRS}}(\mathbf{q}) \right|^2 \delta(\hbar\omega_i - \hbar\omega_f - \hbar\Omega_{\mathrm{LO}}), \tag{6}$$

where ω_f is the scattered light frequency. In PL processes additional exciton scattering by acoustic phonons takes place. The detailed theory of the DRRS and PL is presented in Sec. III E; here we just note that the selection rules for RRS and PL are essentially the same. Thus, to analyze the relative intensities of the DRRS processes for cases A and C [Fig. 4(b)] we need to consider corresponding exciton-phonon scattering matrix elements.

B. Hole-phonon interaction: Case A

In case A the ingoing resonance is X_{lh} in σ^- polarization, and the outgoing resonance is X_{hh} in σ^+ polarization. In this case, following from Eqs. (3), the electron state does not change, while the hole state is changed from the light one, $J_z = -1/2$, to the heavy one, $J_z = 3/2$. As a result, the corresponding hole transition matrix element $V_{\mathrm{hh \leftarrow lh}}^{\mathrm{LO}}$ is proportional to the optical deformation potential constant d_o (or $d_{5o}/\sqrt{2}$) introduced in Refs. [13–15]:

$$V_{\mathrm{hh \leftarrow lh}}^{\mathrm{LO}} = \frac{d_o}{a_0} \sqrt{\frac{\hbar}{2\rho\mathcal{V}\Omega_{\mathrm{LO}}}} \frac{q_z}{q} \mathcal{F}_{\mathrm{hh \leftarrow lh}}(\mathbf{q}), \tag{7}$$

where a_0 is the lattice constant and we use the notations of Ref. [14] for the matrix elements, $\mathcal{V}$ is the normalization volume, and $\mathcal{F}_{\mathrm{hh \leftarrow lh}}(\mathbf{q})$ is the form factor defined by the exciton envelope functions:

$$\mathcal{F}_{\mathrm{hh \leftarrow lh}}(\mathbf{q}) = \int d\mathbf{r}_e d\mathbf{r}_h e^{i\mathbf{q}\mathbf{r}_h} \Phi_n^*(\mathbf{r}_e, \mathbf{r}_h)\Phi_m(\mathbf{r}_e, \mathbf{r}_h). \tag{8}$$

For $\mathbf{q} \to 0$ the form factor is reduced to a constant (~ 1) sensitive to the shape of the envelope functions, and for $q \gg R^{-1}$, where R is the characteristic exciton localization radius, $\mathcal{F}_{\mathrm{hh \leftarrow lh}}(\mathbf{q})$ is decreased to zero.

C. Exchange interaction in the exciton: Case C

For case C the initial and final states belong to the heavy hole exciton X_{hh}, with the former being active in the σ^- polarization and the latter active in the σ^+ polarization. One of the possible scenarios enabling the DRRS in that case is a simultaneous spin flip of both the electron and the hole governed by a combination of the exciton scattering by the LO phonon and the long-range exchange interaction between the electron and the hole [8,16]. The corresponding matrix element in the resonant case, where $\hbar\Omega_{\mathrm{LO}}$ is approximately equal to both $E_m - E_n$ in Eq. (5) and the exciton Zeeman splitting, under the assumption of the Fröhlich interaction, can be recast as [16]

$$V_{\mathrm{hh \leftarrow hh}}^{\mathrm{LO,lr}} = \frac{V_m^{\mathrm{exc}} - V_n^{\mathrm{exc}}}{\Omega_{\mathrm{LO}}} i \sqrt{\frac{2\pi e^2 \hbar\Omega_{\mathrm{LO}}}{\mathcal{V}\varepsilon_*}} \frac{1}{q} \mathcal{F}_{\mathrm{hh \leftarrow hh}}(\mathbf{q}), \tag{9}$$

where $V_{m,n}^{\mathrm{exc}}$ is the matrix element of the electron-hole flip-flop process

$$(1/2, -3/2) \to (-1/2, 3/2),$$

caused, e.g., by the long-range exchange interaction [17]; $\varepsilon_*^{-1} = \varepsilon_\infty^{-1} - \varepsilon_0^{-1}$, with ε_∞ and ε_0 being the high- and low-frequency dielectric constants; and the form factor

$$\mathcal{F}_{\mathrm{hh \leftarrow hh}}(\mathbf{q}) = \int d\mathbf{r}_e d\mathbf{r}_h (e^{i\mathbf{q}\mathbf{r}_e} - e^{i\mathbf{q}\mathbf{r}_h}) \Phi_n^*(\mathbf{r}_e, \mathbf{r}_h)\Phi_m(\mathbf{r}_e, \mathbf{r}_h). \tag{10}$$

In accordance with the analysis of Refs. [8,16] this process is quite weak. The reasons are as follows: (i) Electric neutrality of the excitons results in significant suppression of the Fröhlich interaction, and (ii) the process (9) is already a second-order process compared to the first-order effect in Eq. (7) responsible for case A.

An alternative scenario for line C which does not suffer from the above deficiencies is realized by accounting for the short-range exchange interaction that mixes heavy and light excitonic states active in the same polarization. The corresponding contribution to the Hamiltonian written in the spherical approximation has the form

$$\hat{U}^{\rm sr} = -\tfrac{2}{3} a_0^3 \delta(\boldsymbol{r}_{\rm e} - \boldsymbol{r}_{\rm h}) \mathcal{E}_0 \boldsymbol{\sigma} \cdot \boldsymbol{J}. \tag{11}$$

Here $\mathcal{E}_0$ is the exchange interaction parameter, $\boldsymbol{\sigma}$ are the electron spin-Pauli matrices, and $\boldsymbol{J}$ is the hole angular momentum 3/2 operator. Symmetry considerations together with the microscopic analysis show that the following matrix element is nonzero:

$$U^{\rm sr} = \langle \sigma_{\rm lh}^- | \hat{U}^{\rm sr} | \sigma_{\rm hh}^- \rangle. \tag{12}$$

Accounting for this interaction and for the LO phonon emission, we obtain the matrix element of the $\sigma_{\rm hh}^- \to \sigma_{\rm hh}^+$ transition in the form

$$V_{\rm hh \leftarrow hh}^{\rm LO,sr} = \frac{V_{\rm hh \leftarrow lh}^{\rm LO} U^{\rm sr}}{E_{\sigma_{\rm hh}^-} - E_{\sigma_{\rm lh}^-}}. \tag{13}$$

Here $V_{\rm hh \leftarrow lh}^{\rm LO}$ is the matrix element (7), and the energy difference $E_{\sigma_{\rm hh}^-} - E_{\sigma_{\rm lh}^-} = \Delta E_{\rm hh,-3/2} - \Delta E_{\rm lh,-1/2} - \Delta_{\rm hh-lh}$. We note that the absolute value of this matrix element is by far larger than that of $V_{\rm hh \leftarrow hh}^{\rm LO,lr}$ in Eq. (9) for two reasons: There is no cancellation of the exchange interaction contributions since $|E_{\sigma_{\rm hh}^-} - E_{\sigma_{\rm lh}^-}| \ll \hbar\Omega_{\rm LO}$ in the experimental configuration, and $|\mathcal{F}_{\rm hh \leftarrow lh}| \gg |\mathcal{F}_{\rm hh \leftarrow hh}|$.

D. Spin-conserving RRS: Case B

Let us briefly discuss the mechanisms behind the spin-conserving transition marked as B in Fig. 4(b). This transition is expected to occur in the $z(\sigma^+, \sigma^+)\bar{z}$ configuration, where the light hole exciton is excited in the initial state and the heavy hole exciton is formed after the LO phonon emission.

A possible scenario for this process is short-range mixing of the cocircularly polarized light and heavy hole excitons (11) and subsequent spin-conserving heavy hole exciton relaxation. This process is assumed to be quite weak owing to Fröhlich interaction suppression for neutral excitons [see the form factor (10) and discussion below that equation]. Note that two independent spin flips, (i) the hole conversion from the light one with $J_z = +1/2$ to the heavy one with $J_z = +3/2$ described by a matrix element similar to $V_{\rm hh \leftarrow lh}^{\rm LO}$ [13–15] and (ii) the electron spin flip, are highly unlikely. As a result, we conclude that from the theoretical standpoint line B should be suppressed compared to both A and C. This is in agreement with experiment, in which such a transition has not been detected.

E. Model of RRS and PL in systems with inhomogeneous broadening

Usually, the distinction between RRS of light mediated by excitons and excitonic PL in semiconductors is rather complicated and, in many cases, impossible [18,19]. However, in structures with significant inhomogeneous broadening these two processes can be separated. In the case of RRS the emission (scattered) line is always shifted with respect to the incident (excitation) laser line by a fixed amount of energy, in our case the optical phonon energy. In other words, the
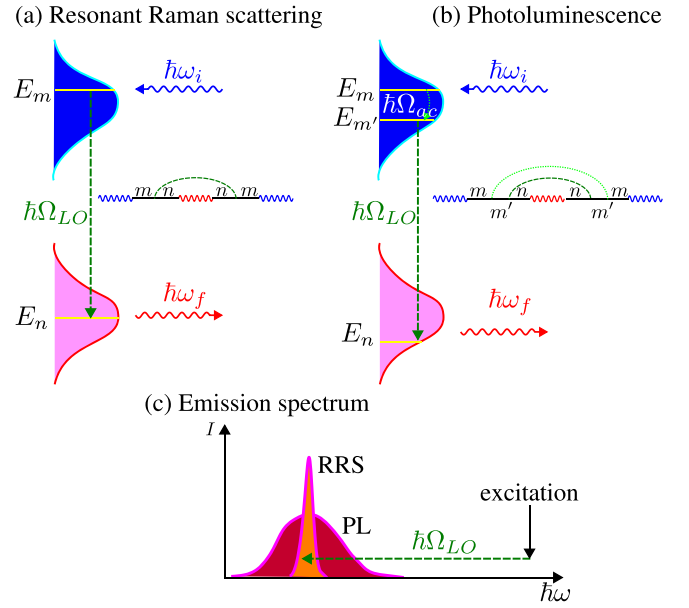

FIG. 5. Schematic illustration of emission processes. (a) Resonant Raman scattering, where only one optical phonon is involved. (b) Photoluminescence, where additional acoustic phonon scattering takes place. (c) Resulting emission spectrum, which is a superposition of the resonant Raman scattering and photoluminescence. Insets show corresponding diagrams.

RRS line follows the excitation laser, which is seen in Fig. 1. As schematically shown in Fig. 5(a), in the RRS process the photoexciton emits an optical phonon, scattering to the final state, and then recombines with the photon emission before any additional inelastic or quasielastic scattering by the acoustic phonon takes place. By contrast, in the case of PL the energy position of the emission band does not follow the excitation laser energy. In the simplest possible model, in the case of PL the exciton resonantly created by the laser (or after emission of the optical phonon) emits and absorbs one or several acoustic phonons hopping over the localized states in an inhomogeneous ensemble [Fig. 5(b)]. Additionally, the PL can be contributed by a variety of scattering processes without direct involvement of the LO phonon, e.g., by the exciton relaxation mediated by acoustic phonons.

It is convenient to describe the emission of the structure within the Green's function approach that allows us to take into account both coherent Raman scattering of light and incoherent PL. To that end we follow Refs. [20,21] and calculate the self-energy of the incident photon with frequency $\hbar\omega_i$ related to the scattering into the final state with frequency $\hbar\omega_f$ (see the insets in Fig. 5).

F. Resonant Raman scattering

In the case of RRS only one exciton-phonon interaction process is involved, and the transition rate can be recast as [see inset in Fig. 5(a)]

$$W^{\rm RRS} = C \sum_{mn,\boldsymbol{q}} \left| M_n M_m V_{nm}^{\rm LO}(\boldsymbol{q}) \right|^2 |G_n(\hbar\omega_f)|^2$$

$$\times |G_m(\hbar\omega_i)|^2 D_{\rm LO,\boldsymbol{q}}(E_m - E_n). \tag{14}$$

Here C is a prefactor that smoothly depends on the frequencies of light, and as before, m and n denote initial and final exciton states, $M_{n,m}$ are the corresponding light-exciton coupling matrix elements, and $V_{nm}^{LO}(\boldsymbol{q})$ is the exciton-LO-phonon interaction matrix element as specified in Secs. III B and III C. The exciton Green's functions

$$G_n(\varepsilon) = \frac{1}{\varepsilon - E_n + i\gamma_n}, \qquad (15)$$

where E_n are the energies of the involved states and γ_n are their dampings caused by all possible scattering processes. In what follows we assume that the inhomogeneous broadening is sufficiently larger than γ_n; thus, we replace the Lorentzians by Dirac δ functions as follows:

$$|G_n(\varepsilon)|^2 = \frac{\pi}{\gamma_n}\delta(\varepsilon - E_n). \qquad (16)$$

Similarly, the phonon Green's function in the absence of the phonon damping reads

$$D_{LO,\boldsymbol{q}}(\varepsilon) = \pi\delta[\varepsilon - \hbar\Omega_{LO}(\boldsymbol{q})]; \qquad (17)$$

see Refs. [20,21] for further details.

For further estimations and comparison with photoluminescence it is instructive to assume that in the relevant range of phonon momenta and involved states (n,m) where $V_{nm}^{LO}(\boldsymbol{q})$ is significant, light-matter coupling matrix elements M_n and M_m and damping rates γ_n and γ_m do not depend on the energy of the state. Similarly, we assume, for these relevant states, a constant matrix element of the exciton-phonon coupling:

$V_{nm}^{LO}(\boldsymbol{q}) = V^{LO}$. As a result we have

$$W^{RRS} = \frac{C\pi^3}{\gamma_n\gamma_m}\mathcal{D}_m(\hbar\omega_i)\mathcal{D}_n(\hbar\omega_f)|M_nM_mV^{LO}|^2$$
$$\times\,\delta(\hbar\omega_i - \hbar\omega_f - \hbar\Omega_{LO}), \qquad (18)$$

where $\mathcal{D}_m(\varepsilon)$ and $\mathcal{D}_n(\varepsilon)$ are the effective densities of states for the initial and final excitonic states. Equation (18) can be recast in a somewhat different form introducing the rate of the optical phonon emission

$$W_{LO} = 2\pi|V^{LO}|^2\mathcal{D}_n(\hbar\omega_f) \qquad (19)$$

as

$$W^{RRS} = \frac{C\pi^2}{2\gamma_n\gamma_m}\mathcal{D}_m(\hbar\omega_i)|M_nM_m|^2$$
$$\times\,W_{LO}\delta(\hbar\omega_i - \hbar\omega_f - \hbar\Omega_{LO}). \qquad (20)$$

Equation (20) is the key result of this part. It shows that for RRS the frequencies of the incident and secondary photons are connected: $\hbar\omega_f = \hbar\omega_i - \hbar\Omega_{LO}$.

G. Photoluminescence

In order to describe incoherent photoluminescence the Green's function method can also be used. In that case we need to take into account additional acoustic phonon scattering of the exciton. For simplicity, we consider the acoustic phonon scattering for only excited states. To begin with, we assume that only one additional acoustic phonon is emitted or absorbed before the LO phonon emission. Thus, in agreement with the inset in Fig. 5(b) the PL rate reads

$$W^{(1)} = C\sum_{\substack{m,n,\\\boldsymbol{q},\boldsymbol{Q},\pm}}\left|M_nM_mV_{nm}^{LO}(\boldsymbol{q})\right|^2|G_n(\hbar\omega_f)|^2|G_m(\hbar\omega_i)|^2\pi\left|V_{m'm}^{ac}(\boldsymbol{Q})\right|^2|G_{m'}(\hbar\omega_i \mp \hbar\Omega_{ac,\boldsymbol{Q}})|^2D_{LO,\boldsymbol{q}}(E_{m'} - E_n). \qquad (21)$$

Here the signs $\pm$ refer to the emission or absorption of the acoustic phonon with the momentum $\boldsymbol{Q}$ and dispersion $\Omega_{ac}(\boldsymbol{Q})$, and $V_{m'm}^{ac}(\boldsymbol{Q})$ is the exciton-acoustic-phonon interaction matrix element describing the scattering between states m' and m. In this calculation we neglect the damping of the acoustic phonon. Introducing, by analogy with Eq. (19), the acoustic phonon scattering rate

$$W_{ac} = 2\pi\sum_{\boldsymbol{Q},\pm}\left|V_{m'm}^{ac}(\boldsymbol{Q})\right|^2\delta[E \mp \hbar\Omega_{ac}(\boldsymbol{Q})] \qquad (22)$$

and assuming, as before, that it does not depend on m and m' and energy for the involved states, we can sum over $\boldsymbol{Q}$, $\pm$, and m' in Eq. (21), with the result

$$W^{(1)} = \frac{C\pi^2}{2\gamma_n\gamma_m}\mathcal{D}_m(\hbar\omega_i)|M_nM_m|^2$$
$$\times\,W_{LO}\mathcal{D}_n(\hbar\omega_f)\frac{W_{ac}}{2\gamma_m}. \qquad (23)$$

Equation (23) can be readily extended to allow for processes with multiple acoustic phonons. Summing up the ladder diagrams (cf. Ref. [21]) and noting that each step in the

ladder gives the factor $W_{ac}/(2\gamma_m)$, i.e., the ratio of the acoustic phonon emission/absorption rate to the total out-scattering rate of state m, we obtain, instead of Eq. (23),

$$W^{PL} = \frac{C\pi^2}{2\gamma_n\gamma_m}\mathcal{D}_m(\hbar\omega_i)|M_nM_m|^2$$
$$\times\,W_{LO}\mathcal{D}_n(\hbar\omega_f)\frac{W_{ac}}{2\gamma_m - W_{ac}}. \qquad (24)$$

If the only scattering processes are the acoustic and LO scattering, then $2\gamma_m = W_{ac} + W_{LO}$, and $W_{ac}/(2\gamma_m - W_{ac}) = W_{ac}/W_{LO}$.

IV. DISCUSSION

Analysis of the experimental result shown in Fig. 3(b) gives the ratio between the efficiencies of the DRRS process for case A and case C. We use a sum of two Lorentz contours to fit the data and find that the ratio of the amplitudes for the two cases is 3 when the ratio of the integral areas of these contours reaches 10. From the theory, the ratio between the intensities of the DRRS process for cases A and C can be estimated from

Eqs. (7) and (13) as follows:

$$\frac{W^{\mathrm{RRS,C}}}{W^{\mathrm{RRS,A}}} \sim \left| \frac{U^{\mathrm{sr}}}{E_{\sigma_{\mathrm{hh}}^-} - E_{\sigma_{\mathrm{lh}}^-}} \right|^2. \tag{25}$$

For the experimental value $E_{\sigma_{\mathrm{hh}}^-} - E_{\sigma_{\mathrm{lh}}^-} \approx 8$ meV in $B = 0.65$ T and the estimate $|U^{\mathrm{sr}}| \sim 1\text{–}2$ meV it follows that this ratio is much smaller than unity. Physically, this occurs because the additional spin-flip process needed in case C is weak.

The ratio between the integral intensity of RRS with LO phonon emission and the integral intensity of the inhomogeneous PL is found to be 0.15 in the case of the double resonance conditions in case A and 0.03–0.05 for the non-resonance case and case C. The ratio of the integral RRS and PL intensities can be theoretically estimated by making use of Eqs. (20) and (24), which yield

$$\frac{W^{\mathrm{RRS}}}{W^{\mathrm{PL}}} \sim \frac{W_{\mathrm{LO}}}{W_{\mathrm{ac}}}. \tag{26}$$

This ratio is smaller than unity because the LO phonon emission probability is suppressed due to exciton neutrality or because additional electron spin-flip processes are necessary.

Note that the developed approach that simultaneously accounts for RRS and PL does not allow us to precisely describe the PL line shape. Indeed, at the low temperatures relevant for the experiment, almost no PL signal at energies above the LO phonon RRS line is expected due to suppressed acoustic phonon absorption. Hence, to describe the PL we assume additional channels of exciton relaxation and light-heavy exciton conversion caused by exciton-acoustic phonon interaction. In that case, the heavy-light exciton conversion can be assisted by the off-diagonal momentum-dependent terms in the Luttinger Hamiltonian. In such a mechanism, naturally, the energy of the exciton is lost in small portions, and the PL emission spectrum roughly corresponds to the heavy-exciton density of states. Even in this case, Eq. (26) can be used as a lower bound for the RRS intensity since RRS is controlled by the optical phonon emission and PL requires an acoustic phonon scattering.

V. SUMMARY

We have experimentally and theoretically studied the efficiencies of the double resonant Raman scattering in the quantum well of the diluted magnetic semiconductor (Cd, Mn)Te/(Cd, Mg)Te between different states of the exciton. Due to the presence of the giant Zeeman effect in the DMS it was possible to tune the energies of the exciton states over a wide range by applying a moderate magnetic field in the Faraday geometry. It was observed that DRRS with LO phonon emission is the most efficient when the ingoing resonance is the light hole exciton state with an angular momentum projection of -1 and the outgoing resonance falls in the heavy hole exciton state with a projection of $+1$ (case A). It was shown that only the change in the angular momentum projection of the hole is necessary for this process to take place, while the electron state does not change. The DRRS process between the states of the heavy hole exciton with different angular momentum projections (case C) was observed to be 3–10 times less efficient than the previous case. It was shown that for this process to occur one also needs to take into account the exchange interaction between the electron and hole in the exciton to accommodate simultaneous spin flips of both the electron and the hole, making such transitions weaker. Although polarization conserving light-to-heavy hole exciton transition in the DRRS process is not forbidden (case B), it is much weaker than for both cases A and C.

Finally, we compared the integral intensities of the resonance Raman scattering line and the inhomogeneously broadened PL. We found that under the conditions of case A in the DRRS process the ratio is 0.15, whereas under the other resonance conditions or off resonance this ratio is 0.03–0.05. The smallness of the ratio could be explained by the suppression of the probability of the LO phonon emission.

[1] R. Gontijo, G. Resende, C. Fantini, and B. Carvalho, Double resonance Raman scattering process in 2D materials, J. Mater. Res. **34**, 1976 (2019).

[2] N. B. Shinde and S. K. Eswaran, Davydov splitting, double-resonance Raman scattering, and disorder-induced second-order processes in chemical vapor deposited MoS$_2$ thin films, J. Phys. Chem. Lett. **12**, 6197 (2021).

[3] G. Wang, M. M. Glazov, C. Robert, T. Amand, X. Marie, and B. Urbaszek, Double resonant Raman scattering and valley coherence generation in monolayer WSe$_2$, Phys. Rev. Lett. **115**, 117401 (2015).

[4] F. Cerdeira, E. Anastassakis, W. Kauschke, and M. Cardona, Stress-induced doubly resonant Raman scattering in GaAs, Phys. Rev. Lett. **57**, 3209 (1986).

[5] D. A. Kleinman, R. C. Miller, and A. C. Gossard, Doubly resonant LO-phonon Raman scattering observed with GaAs-Al$_x$Ga$_{1-x}$As quantum wells, Phys. Rev. B **35**, 664 (1987).

[6] S. I. Gubarev, T. Ruf, and M. Cardona, Doubly resonant Raman scattering in the semimagnetic semiconductor Cd$_{0.95}$Mn$_{0.05}$Te, Phys. Rev. B **43**, 1551 (1991).

[7] D. R. Yakovlev, W. Ossau, A. Waag, G. Landwehr, and E. L. Ivchenko, Double 2s-1s resonance in LO-phonon-assisted secondary emission of quantum-well structures, Phys. Rev. B **52**, 5773 (1995)

[8] W. M. Chen, I. A. Buyanova, G. Yu. Rudko, A. G. Mal'shukov, K. A. Chao, A. A. Toropov, Y. Terent'ev, S. V. Sorokin, A. V. Lebedev, S. V. Ivanov, and P. S. Kop'ev, Exciton spin relaxation in diluted magnetic semiconductor Zn$_{1-x}$Mn$_x$Se/CdSe superlat-

tices: Effect of spin splitting and role of longitudinal optical phonons, Phys. Rev. B **67**, 125313 (2003).

[9] A. S. Gurin, D. O. Tolmachev, N. G. Romanov, B. R. Namozov, P. G. Baranov, Yu. G. Kusrayev, and G. Karczewski, ODMR evidence of the electron cascade in multiple asymmetrical (CdMn)Te quantum wells, JETP Lett. **102**, 230 (2015).

[10] A. V. Komarov, S. M. Ryabchenko, O. V. Terletskii, I. I. Zheru, and R. D. Ivanchuk, Magneto-optical studies and double optic-magnetic resonance of exciton band in CdTe: Mn2+, Soviet J. Exp. Theoretical Phys. **46**, 318 (1977).

[11] S. I. Gubarev, Free and bound exciton in II-VI semimagnetic compounds, J. Cryst. Growth **101**, 882 (1990).

[12] V. D. Kulakovskii, M. G. Tyazhlov, S. I. Gubarev, D. R. Yakovlev, A. Waag, and G. Landwehr, Magnetic-field-induced dissociation of bound excitons in semi-magnetic semiconductor quantum wells, Nuovo Cimento D **17**, 1549 (1995).

[13] G. L. Bir and G. E. Pikus, Theory of the deformation potential for semiconductors with a complex band structure, Sov. Phys. Solid State **2**, 2039 (1961).

[14] W. Pötz and P. Vogl, Theory of optical-phonon deformation potentials in tetrahedral semiconductors, Phys. Rev. B **24**, 2025 (1981).

[15] R. Scholz, Hole-phonon scattering rates in gallium arsenide, J. Appl. Phys. **77**, 3219 (1995).

[16] E. Tsitsishvili, R. v. Baltz, and H. Kalt, Phonon-induced exciton spin relaxation in semimagnetic quantum wells, Phys. Rev. B **71**, 155320 (2005).

[17] In Refs. [8,16] excitons were assumed to propagate freely in the quantum well plane. For excitons localized on anisotropic potential fluctuations a similar effect is possible [22,23].

[18] P. Y. Yu and M. Cardona, *Fundamentals of Semiconductors* (Springer, Berlin, 2010).

[19] E. L. Ivchenko, *Optical Spectroscopy of Semiconductor Nanostructures* (Alpha Science, Harrow, UK, 2005).

[20] E. L. Ivchenko, I. G. Lang, and S. T. Pavlov, Resonant secondary radiation in polar semiconductors, Phys. Status Solidi B **85**, 81 (1978).

[21] I. Paradisanos, G. Wang, E. M. Alexeev, A. R. Cadore, X. Marie, A. C. Ferrari, M. M. Glazov, and B. Urbaszek, Efficient phonon cascades in WSe_2 monolayers, Nat. Commun. **12**, 538 (2021).

[22] M. Z. Maialle, Spin dynamics of localized excitons in semiconductor quantum wells in an applied magnetic field, Phys. Rev. B **61**, 10877 (2000).

[23] S. V. Gupalov, E. L. Ivchenko, and A. V. Kavokin, Fine structure of localized exciton levels in quantum wells, Fine structure of localized exciton levels in quantum wells, J. Exp. Theor. Phys. **86**, 388 (1998).